Pergamon

Int. J. Heat Mass Transfer. Vol. 37, No. 6, pp. 955–965, 1994
Copyright © 1994 Elsevier Science Ltd
Printed in Great Britain. All rights reserved
0017-9310/94 $6.00 + 0.00

0017-9310(93)E0008-5

Maximum and mean droplet sizes in annular two-phase flow

G. KOCAMUSTAFAOGULLARI, S. R. SMITS and J. RAZI

Department of Mechanical Engineering, University of Wisconsin-Milwaukee, Milwaukee, WI 53201, U.S.A.

(*Received* 8 *February* 1993 *and in final form* 6 *October* 1993)

Abstract—The initial drop size in an annular flow which is determined in terms of the mechanism of droplet generation by shearing off of roll-wave crests by gas flow can be larger than the maximum stable droplet size in forced convection pipe flow. In this case the droplet size is further determined by droplet disintegration mechanism. Disintegration of droplets in a gas stream has been studied by a number of researchers. Several disruptive mechanisms of droplet break-up have been suggested. Each of these controlling mechanisms was evaluated as applied to the annular flow. It was concluded that in a case of partial entrainment the maximum size of a fluid particle was mainly controlled by the action of the dynamic force a fluid particle experiences in a relative motion. Based on this dynamic force and the stabilizing effect of surface tension, a detailed method for predicting the maximum droplet size in annular flow was presented. The correlations for the representative droplet mean diameters as well as the size distribution were then developed. A comparison with experimental data covering a wide range of fluid and flow variables indicated that indeed the postulated droplet disintegration mechanism was the dominant factor in determining the drop size.

INTRODUCTION

THE INITIAL droplet size in an annular flow is determined in terms of the mechanism of droplet generation such as shearing off of roll-wave crests forming on a thin liquid film by a streaming gas flow, Kataoka *et al.* [1]. From annular flow visualization studies of Whalley *et al.* [2], it was observed that the droplets emerge from a roll-wave. However, the largest droplets with a diameter larger than the maximum stable size start oscillating for a while, and suddenly, irrespective of their position in the tube cross-section, a higher frequency oscillation starts that results in the break-up of the droplet in a short period of time. Lopes and Dukler's [3] local droplet size measurements confirmed qualitative observations of Whalley *et al.* that the average drop size decreases towards the center of the annular two-phase flow column. These experimental findings are a clear indication that the droplet size in an annular flow is not determined at the time of entrainment. It is mainly controlled by the mechanics of the gas–droplet interaction in the turbulent gas stream.

For the purpose of providing basic information on the maximum size a droplet can reach, a number of processes which may cause break-up of droplets in a gas flow have been studied by several investigators, and a number of disruptive force mechanisms of the droplet break-up have been identified in the literature. Each of these controlling mechanisms was tested by Lopes and Dukler [3] against their experimental air/water data. It was concluded that the maximum droplet size in an annular flow is mainly controlled by the action of forces resulting from the pressure fluctuations of the turbulent flow of the gas around a droplet. Based on the theory presented by Kolmogorov [4], Lopes and Dukler suggested a simple predictive method for the droplet size. The method incorporated a critical Weber number of 0.194 determined from their air/water data at about atmospheric conditions. In the present study, the Sauter mean droplet sizes predicted by the Lopes and Dukler method were compared using the recent data of Jepson *et al.* [5, 6], where the property effects such as the surface tension and the fluid density ratios were investigated systematically. The method gave a reasonably good estimate of droplet sizes for those data where the density ratios are comparable to the atmospheric air/water system. However, differences between predictions and the experimental data became larger and larger as the density ratio moves away from the air/water density ratio of atmospheric conditions.

In view of the above comparison, an investigation has been undertaken to clarify the property effects on the droplet disintegration in an annular flow. This paper which summarizes our findings has three objectives. Based on the competing forces between stabilizing surface stresses and the disruptive dynamic force exerted on a particle partially entrained by the surrounding fluids, the first objective is to develop a method to describe the break-up of entrained droplets in the gas core of an annular flow. The second objective is to develop an experimentally based simple correlation for the maximum stable size a droplet can reach in a turbulent flow field. Finally, the third objec-

NOMENCLATURE

a_w	roll wave amplitude
C_g	coefficient in equation (16)
C_w	coefficient defined by equation (15)
d	spherical droplet diameter
d_h	hydraulic diameter of flow channel
d_{max}	maximum spherical bubble diameter
d_{sm}	Sauter mean diameter of droplets ($\equiv d_{32}$)
d_{vm}	volume median diameter of droplets
j	superficial velocity
K	dimensionless quantity defined by equation (19)
p	pressure
Re_f	liquid Reynolds number ($\equiv \rho_f d_h \langle j_f \rangle / \mu_f$)
Re_g	gas Reynolds number ($\equiv \rho_g d_h \langle j_g \rangle / \mu_g$)
u	velocity
$\overline{u_c'^2}$	mean square fluctuation velocity difference between two points at a distance d_{max}
$u_{r)max}$	maximum value of local relative velocity
We_{cr}	critical Weber number
We_m	modified Weber number
z	axial coordinate.

Greek Symbols

δ	average liquid film thickness
$\Delta\rho$	density difference
ε	energy dissipation rate per unit mass
η	distribution parameter in upper limit, log–normal distribution
λ	scale of local turbulence
μ	dynamic viscosity
ξ	parameter defined by equation (31)
ρ	density
σ	surface tension
τ	external stresses
τ_i	interfacial shear stress
υ	normalized volume of droplet in distribution.

Subscripts

c	continuous phase
d	dispersed phase
f	liquid phase
g	gas phase.

Symbols

$\langle\ \rangle$	area-averaged value.

tive is to extend the maximum droplet size predictions to obtain the droplet size distribution as well as mean droplet sizes.

MECHANISTIC MODELING OF DROPLET BREAK-UP

A generalized break-up mechanism can be expressed as a balance between external stresses, τ, and the surface stress, $\sigma/(d/2)$, where σ is the surface tension and d is the droplet diameter. These stresses influence both the size of droplets which are torn away from their point of formation and also the maximum droplet size which is stable in the flow field. Therefore, the stability condition can be characterized by the ratio of the external stresses and surface stress by a suitably chosen Weber number. The critical Weber number above which the droplet is no longer stable is defined as

$$We_c \equiv \frac{\tau d_{max}}{2\sigma} \tag{1}$$

where d_{max} is the maximum stable droplet size.

Basically there are two external disruptive stresses that are involved in the breaking up of particles, namely, viscous and dynamic stresses. The relative order of magnitude of these stresses is determined by the ratio of length scales, d_{max}/λ, where λ is the internal length scale of local turbulence for the equilibrium range (usually called the Kolmogorov microscale). When $d_{max} \leqslant \lambda$ viscous forces play a dominant role. In this case, the phenomena associated with the break-up of a drop or bubble are similar to those investigated by Taylor [7]. In most applications, the particle Reynolds numbers which are characteristic of the internal flow field are much greater than unity so viscous effects are negligible. In this case, the disruptive dynamic forces and stabilizing surface tension are dominant in the process of fluid particle break-up.

The disruptive forces may develop either through the local relative motion around the droplet, or through the changes in eddy velocities over the length of a droplet. For both cases, however, the external stress appearing in equation (1) can be expressed in terms of the kinetic energy differences around the droplet. From equation (1), the former yields

$$We_{cr)1} = \rho_c u_{r)max}^2 d_{max}/2\sigma \tag{2}$$

whereas the latter gives

$$We_{cr)2} = \rho_c \overline{u_c'^2} d_{max}/2\sigma. \tag{3}$$

The mean-square spatial fluctuating velocity term, $\overline{u_c'^2}$, describes the turbulent pressure forces of eddies of size d_{max} and is defined as the average of the square of the differences in velocity over a distance equal to the fluid particle diameter. $u_{r)max}$ is that limiting local relative velocity at which a fluid will flow around a particle suspended in it. The subscript c identifies the continuous phase.

Considering the simplest case of turbulence,

namely, an isotropic homogeneous turbulence, the main contribution to the kinetic energy, $\overline{u_c'^2}$, is made by the fluctuations in the region of wavelength where the Kolmogorov energy distribution is valid. In this region the local turbulence pattern is solely determined by the energy dissipation rate per unit mass, ε. The mean square velocity difference, $\overline{u_c'^2}$, between two points, d_{max}, is given by Batchelor [8] as follows:

$$\overline{u_c'^2} \sim (\varepsilon d_{max})^{2/3} \tag{4}$$

whereas $u_{r)max}$ is given by Levich [9] as

$$u_{r)max} \sim [\varepsilon d_{max}(\rho_d/\rho_c)]^{1/3}(|\Delta\rho|/\rho_d)^{1/2} \tag{5}$$

where the subscript d identifies the dispersed phase.

When equations (4) and (5) are inserted into their respective places in equations (2) and (3), the following critical Weber numbers can be obtained:

$$We_{cr)2} = k_2\rho_c\varepsilon^{2/3}d_{max}^{5/3}/\sigma \tag{6}$$

and

$$We_{cr)1} = k_1\rho_c\varepsilon^{2/3}d_{max}^{5/3}(\rho_d/\rho_c)^{2/3}(|\Delta\rho|/\rho_d)/\sigma \tag{7}$$

where k_1 and k_2 are proportionality coefficients. The numerical coefficients probably have no great significance. They are set forth here only in order to stress the absence in these formulas of large numerical coefficients. Both k_1 and k_2 are the same order of one.

Equations (6) and (7) can be used to determine the maximum fluid particle size as follows:

$$d_{max} = (\sigma We_{cr)2}/k_2\rho_c)^{3/5}\varepsilon^{-2/5} \tag{8}$$

and

$$d_{max} = (\sigma We_{cr)1}/k_1\rho_c)^{3/5}\varepsilon^{-2/5}(\rho_c/\rho_d)^{2/5}(\Delta\rho/\rho_d)^{-3/5}. \tag{9}$$

Both equations relate the maximum stable bubble or drop diameter to the energy dissipation rate of ε and the surface tensions but differ in their functional dependence on the fluid densities. These equations have previously been used to describe liquid–liquid and gas–liquid dispersions in horizontal pipelines, but their application to liquid–gas droplet systems has not been evaluated for a wide range of fluid properties. Sevik and Park [10] were able to predict, theoretically, the value of $We_{cr)2} = 1.24$ for the air bubbles in a water jet and $We_{cr)2} = 0.52$ for the case of liquid droplets in turbulent liquid of equal density. These numerical values of the critical Weber number are remarkably good for the air/water bubbly flow experimental observations of Sevik and Park and for the liquid–liquid dispersions experiments of Hinze [11]. As mentioned above, however, $We_{cr)2} = 0.194$ obtained for water droplets in turbulent air stream by Lopes and Dukler [3] does not give good results in the whole experimental range of Jepson *et al.* [5, 6], where the density ratio ranged from $\rho_d/\rho_c = 550$ to 3700. The discrepancy can be explained by comparing the expression for fluid velocity relative to the particle, $u_{r)max}$, with the change in velocity of turbulence eddies over a distance equal to the dimension d_{max} of the particle, $(\overline{u_c'^2})^{1/2}$.

A comparison of equations (4) and (5) shows, that, when $\rho_d \leqslant \rho_c$ (gas bubbles or lighter liquid droplets in a surrounding liquid), $u_{r)max} \ll (\overline{u_c'^2})^{1/2}$. In this case, large-scale eddies of continuous phase completely entrain the fluid particle together with portions of fluid adhering to it, and transfer both as a single unit. The entrainment of particles by turbulent eddies is complete. Therefore, the second Weber number criterion, $We_{cr)2}$, which is based on $\overline{u_c'^2}$, mechanistically describes the fragmentation of drops and bubbles in a turbulent liquid flow for $\rho_d \leqslant \rho_c$.

However, the disintegration of a drop in a turbulent gas stream, i.e. where the density of the medium is low as compared to that of the liquid within the drop, occurs in a somewhat different way. In this case, the entrainment of particles by turbulence eddies cannot be complete. The smaller-scale fluid motions are unable to entrain the particle, and in relation to them, the particle acts as a motionless solid body. The fluid participating in these small-scale motions flows over the surface of the particle. In this case, the local relative velocity given by equation (5) plays an important role in the mechanism of the drop's disintegration. In the case of $\rho_d \gg \rho_c$, from equations (4) and (5) it is evident that

$$u_{r)max}/(\overline{u_c'^2})^{1/2} \simeq (\rho_d/\rho_c)^{1/3} \tag{10}$$

which indicates that $u_{r)max}^2 \gg \overline{u_c'^2}$. Therefore, the disruptive forces based on $u_{r)max}$ become much larger than the disruptive forces generated by changes in eddies. In this case, the first critical Weber number criterion $We_{cr)1}$, describes the disintegration of drops in a turbulent gas stream. This is the mechanistic approach that will be taken in the remaining part of this paper.

MAXIMUM DROPLET SIZE CORRELATION

In view of the above discussion, equation (9) describes the maximum droplet size in an annular flow as a function of the local energy dissipated by the turbulence and the physical properties of the fluids. Considering the fact that $\rho_d \gg \rho_c$, equation (9) can be simplified as follows:

$$d_{max} = (\sigma We_{cr)1}/k_1\rho_g)^{3/5}(\rho_g/\rho_f)^{2/5}\varepsilon^{-2/5} \tag{11}$$

where the subscripts c and d identifying the continuous and dispersed phase, respectively, are replaced by the subscripts f and g for the liquid and gaseous phases.

In a pipeline the local energy dissipation rate, ε, is equal to the average energy dissipation rate, $\langle\varepsilon\rangle$, and approximated by Lopes and Duckler [3] as follows:

$$\langle\varepsilon\rangle \simeq (\langle j_g\rangle/\rho_g)(-dP/dz)_f = (\langle j_g\rangle/\rho_g)(4\tau_i/d_h) \tag{12}$$

where $\langle j_g\rangle$, $(-dP/dz)_f$, τ_i and d_h, respectively, are the

average superficial gas velocity, frictional component of the axial pressure gradient, interfacial shear and the hydraulic diameter of flow channel. With equation (12) for ε, the maximum stable droplet size can be calculated from equation (11) as follows:

$$d_{max} = We_{cr)1}^{3/5}(\sigma/k_1\rho_g)^{3/5}(\rho_g/\rho_f)^{2/5} \times [(\langle j_g\rangle/\rho_g)(4\tau_i/d_h)]^{-2/5}. \quad (13)$$

Ishii and Grolmas [12] slightly modified Wallis' [13] interfacial shear correlation, and derived the following expression for the annular flow.

$$\tau_i = 0.0428(C_gC_w)^{2/3}Re_f^{1/6}Re_g^{-2/3}(\rho_g/\rho_f)^{1/3} \times (\mu_f/\mu_g)^{2/3}(\rho_g\langle j_g\rangle^{2/2}) \quad (14)$$

where C_g is a constant coefficient, and C_w is given in terms of the viscosity number as follows:

$$C_w = 1/35.34\,N\mu^{4/5} \quad \text{for } N\mu \leqslant 1/15 \quad (15a)$$

and

$$C_w = 0.25 \quad \text{for } N\mu > 1/15 \quad (15b)$$

where the viscosity number, $N\mu$, is defined by

$$N\mu \equiv \mu_f/[\rho_f\sigma(\sigma/g\Delta\rho)^{1/2}]^{1/2}. \quad (16)$$

Finally, substituting equation (14) into equation (13) for τ_i and rearranging the resulting equation, an expression for the maximum drop diameter can be obtained.

$$d_{max} = 2.673[We_{cr)1}^{3/5}/C_g^{4/15}k_1^{3/5}](\sigma/\rho_g\langle j_g\rangle^2)^{3/5} \times (Re_g^4/Re_f)^{1/15}[(\rho_g/\rho_f)(\mu_g/\mu_f)]^{4/15}d_h^{2/5}. \quad (17)$$

In terms of dimensionless groups, equation (17) can be expressed as follows:

$$d^*_{max} = 2.673[We_{cr)1}^{3/5}/C_g^{4/15}k_1^{3/5}]\,We_m^{3/5} \times (Re_g^4/Re_f)^{1/15}[(\rho_g/\rho_f)(\mu_g/\mu_f)]^{4/15} \quad (18a)$$

or

$$d^*_{max} = 2.673[We_{cr)1}^{3/5}/C_g^{4/15}k_1^{3/5}]K \quad (18b)$$

where K is defined by

$$K \equiv C_w^{-4/15}\,We_m^{3/5}\,(Re_g^4/Re_f)^{1/15}[(\rho_g/\rho_f)(\mu_g/\mu_f)]^{4/15}. \quad (19)$$

In the above equations, d^*_{max} is the dimensionless drop diameter, and We_m is a modified Weber number based on macroscopic variables. They are defined by:

$$d^*_{max} \equiv d_{max}/d_h \quad \text{and} \quad We_m \equiv \rho_g d_h\langle j_g\rangle^2/\sigma. \quad (20)$$

The foregoing expressions describe the maximum droplet size as a function of the liquid and gas phase Reynolds numbers, modified Weber number and the dimensionless physical property groups. For practical applications, the proportionality constant in the above equation should be correlated in collaboration with experimental data.

Several experiments have been carried out to study droplet size distributions in annular two-phase flow [14–17]. Among these available data, only the Lopes and Dukler [3] data were used for the correlation purpose. There are several reasons for this preference. (1) In their study the actual measured maximum drop diameters were listed together with the statistically determined diameter. (2) They carefully distinguished the maximum diameter measurements in the core from those measured close to the interface. (3) Finally, there was no way of assessing the statistical reliability of the values of d_{max} measured experimentally. However, Lopes and Dukler's measured d_{max} values were close to the statistically expected d_{max} values. It is then expected that the values of measured d_{max} represent well the maximum probable diameter within a reasonable accuracy. Figure 1 shows the dimensionless experimental maximum diameter vs a new dimensionless variable, K.

Most of the data in Fig. 1 fall within $\pm 15\%$ of the following correlation

$$d^*_{max} = 2.609C_w^{-4/15}\,We_m^{3/5}\,(Re_g^4/Re_f)^{1/15} \times [(\rho_g/\rho_f)(\mu_g/\mu_f)]^{4/15} \equiv 2.609K. \quad (21)$$

Several observations can be made with respect to equation (21).

(1) The drop size decreases with increasing superficial gas velocity, $d_{max} \sim \langle j_g\rangle^{-14/15}$. Given that the critical Weber number identifies the maximum stable drop size permissible by balancing the disruptive local inertial and stabilizing surface tension forces, increasing the gas velocity will cause a decrease in drop size. The power of $\langle j_g\rangle$ is in line with the previous experimental results of the volume median diameter, $d_{vm} \sim \langle j_g\rangle^{-n}$ where the power n is between 0.8 (Linstead *et al.* [18] and Tatterson [16]), and 1.2 (Wicks and Dukler [14, 15] and Cousins and Hewitt [17]). This tendency is also similar to the experimental results of Jepson *et al.* [5, 6] where the Sauter mean diameter of droplets decreases approximately to the 1.2 power of the gas flux. The above correlation yields a power of $n = 14/15$ which is within the range of previously reported experimental observations.

(2) The drop size slightly decreases with increasing

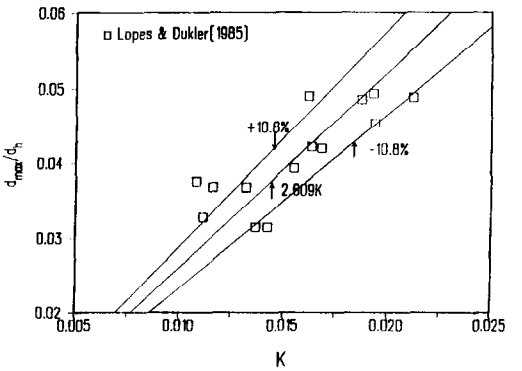

FIG. 1. Maximum diameter vs dimensionless fluid property and flow variable groups.

superficial liquid velocity, $d_{max} \sim \langle j_f \rangle^{-1/15}$. Experimental observations of Cousins and Hewitt [17], Wicks and Dukler [14, 15], Pogson *et al.* [19], Tatterson [16], Azzopardi *et al.* [20–22] and Lopes and Dukler [3] indicate that the average droplet size is almost independent of the liquid flow rate. These experimental observations are consistent with the present correlation where a very weak dependence with a power of $-1/15$ can be found. However, recent experimental observations of Jepson *et al.* [5, 6] indicate that for increasing liquid mass flux, the Sauter mean diameter shows a minimum for the air/water system, continuously decreases with the He/water and increases for the air/CH_3CCl_3 system. Azzopardi *et al.* [22] and Jepson *et al.* related this mean droplet size dependence on the liquid flow rate to the interfacial shear and droplet concentration in the gas core, and, hence, the droplet coalescence resulting in increased droplet size. In the above derivations, none of these effects were considered. Recent experimental observations of Kocamustafaogullari *et al.* [23] for air/water bubbly flow in horizontal pipelines showed a very strong dependence of the mean bubble size with void fraction. These observations are consistent with the hypothesis of refs. [5, 6, 22]. The above derivations leading to the maximum stable size correlation considered a single liquid particle in a gas stream. Presently an analytical study has been initiated to relate the turbulence level to the volumetric concentration of the dispersed phase. Hopefully this study will clarify the above disagreements of the mean droplet size dependence on the liquid flow rate.

(3) Equation (21) indicates that the maximum stable diameter increases with increasing pipe size, $d_{max} \sim d_h^{3/5}$. This is consistent with the experimental observations of Ueda [24] with 10 and 30 mm pipe sizes. However, it contradicts experimental results of Azzopardi *et al.* [20–22], who performed experiments in two different pipe diameters, 22 mm and 125 mm. It is to be noted that at the lower end the pipe sizes of both investigators are comparable. On the other hand, the pipe size used by the latter was much higher than the former although the gas superficial velocities used by both investigators were comparable ($\langle j_g \rangle = 20 \sim 85$ m s^{-1} used by Ueda and $\langle j_g \rangle \simeq 24 \sim 64$ m s^{-1} used by Azzopardi *et al.*). By the time the tube diameter reaches 125 mm many phenomena in gas–liquid flow are altered. For example, the wave structure is changed. It is not surprising, therefore, that results in this large tube diameter show different effects. Drop size measurements with a more systematic pipe size change would be desirable in order to resolve the controversy and to test further the proposed mechanism and the method outlined here to predict droplet size.

(4) Irrespective of whether equation (15a) or (15b) is used for C_w, the maximum stable droplet size from equation (21) varies slightly with the liquid viscosity, and does not depend on the gas viscosity. The viscous forces within the droplet increases its stability, and become important when they are the same order of magnitude as the surface tension forces. By comparing the number mean diameters measured for annular flows by Pogson *et al.* [19] and by Namie and Ueda [25] for liquid viscosities of 0.28 and 1.0 mN s m^{-2}, Tatterson *et al.* [26] found no appreciable influence of liquid viscosity. The agreement with respect to the liquid viscosity dependence is particularly encouraging since the experiments cover a wide range of liquid viscosities.

(5) Finally, comparing equations (18) and (21), one obtains

$$2.673\, We_{cr)1}^{3/5}/C_g^{4/15}k_1^{3/5} = 2.609. \tag{22}$$

The order of magnitude of the critical Weber number can be estimated as follows. According to Kataoka *et al.* [1], the value of C_g is approximately 300 or less. From Levich [9], $k_1 \leqslant 1.0$. Using these values, the critical Weber number can be calculated from equation (22) as

$$We_{cr)1} \leqslant 12.2. \tag{23}$$

Comparing equations (8) and (9) yields

$$We_{cr)2} \simeq k_2(\rho_c/\rho_d)^{2/3}(\Delta\rho/\rho_d)\, We_{cr)1}. \tag{24}$$

For air/water annular flow at about 1.2 atm pressure with $k_2 \simeq 1.0$, which is the value used by Lopes and Dukler [3], equation (24) yields

$$We_{cr)2} \simeq 0.17 \tag{25}$$

which is very close to the value of 0.194 correlated by Lopes and Dukler. Thus, the critical Weber number value based on the Kolmogorov [4] theory is recovered. This suggests that the interfacial shear used in the above derivations was correct for the air/water annular flow although its utility, as discussed in the second section may cause some problems for a wide range of fluid properties.

The maximum stable droplet sizes predicted by equation (21) are compared in Figs. 2(a)–(c), where the liquid Reynolds number is treated as a parameter. Considering the origin of the above correlation coming from the Lopes and Dukler data, a good agreement between the predictions and experimental data of Lopes and Dukler is not surprising. The Cousins and Hewitt data are overpredicted by the present correlation whereas the Wicks data are underpredicted. It is to be noted here that the highest drop sizes appearing in the list of ref. [17] were considered to be the maximum drop sizes in this comparison. As noted above, however, there was no way of assessing the statistical reliability of the values of d_{max} measured experimentally. The data presented in Figs. 2(a)–(c) show no systematic dependence of d_{max} on the liquid flow rate, although the newly developed correlation indicates a weak dependence. Considering the range of data fluctuations in Figs. 2(b)–(c), the agreement between the predictions and experimental measurements is fairly good.

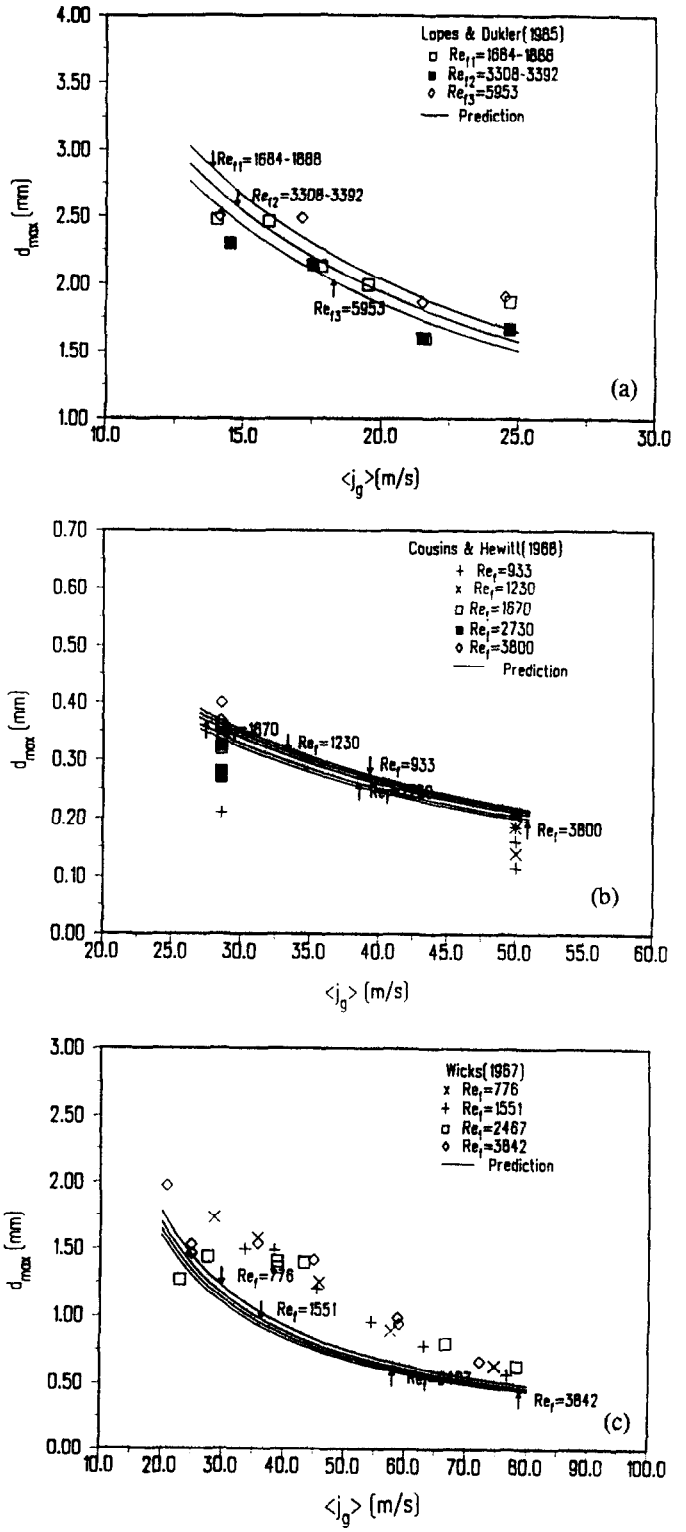

FIG. 2. Theoretical and experimental values of the maximum stable droplet diameter: (a) Lopes and Dukler [3]; (b) Cousins and Hewitt [17]; (c) Wicks [14].

DROPLET SIZE DISTRIBUTION

Volume distribution function

Mugele and Evans [27] analyzed several size distribution formulas for dispersed materials, and their application to spray data. A modification of the log-probability equation, called the upper-limit log-normal distribution equation, was developed and proposed as a standard for describing droplet size distributions in sprays. It introduced a new and physically significant parameter, d_{max}, the maximum stable droplet diameter, for which an expression was developed above.

The upper-limit log-normal distribution advanced by Mugele and Evans for atomizing jets has been used with relative success by several investigators [1, 3, 14–16, 18, 26, 28] in annular dispersed flow. It is given in the following form:

$$\frac{d\upsilon}{d\xi} = (\eta/\sqrt{\pi}) \exp(-\eta^2\xi^2) \tag{26}$$

where υ is the volume fraction of droplets having diameter less than the droplet diameter, d, η is the size distribution parameter, and ξ is the dimensionless function of d defined as

$$\xi = \ln(ad/(d_{max}-d)). \tag{27}$$

The drop size measurements of refs. [3, 14–18] which had a large enough sample size were used to determine a and ξ. The data were fitted to an upper limit, log-normal distribution. Two typical examples of such a fit are illustrated in Figs. 3(a) and (b) for several runs of Lopes and Dukler [3], and Cousins and Hewitt [17]. In these plots, d_{max} represents the maximum expected diameter. The parameters a and η were determined as follows:

$$a = (d_{max}-d_{50})/d_{50} \tag{28}$$

and

$$\eta = \frac{0.394}{\log\left\{\dfrac{[d_{90}/(d_{max}-d_{90})]}{[d_{50}/(d_{max}-d_{50})]}\right\}} \tag{29}$$

where d_{50} and d_{90} are 50th and 90th percentiles which were read from Fig. 3(a).

It is important to notice from Fig. 3(a) that the values of a and η are not completely independent of flow variables. There is a systematic shift on the data points as $\langle j_g \rangle$ varies. Similar shifts can also be observed from Fig. 3(b) as $\langle j_g \rangle$ varies, although the shift is not as consistent as that seen in Fig. 3(a). η and a would be only weakly dependent on flow variables. For practical purposes, they are treated constant in the present study.

The experimental data collected from various sources were analyzed in the same way as shown in Figs. 3(a) and (b) to determine a and η values for each set. Then the results were averaged to obtain $a = 1.93$ and $\eta = 0.75$. Therefore, one obtains a correlation for droplet distribution as

$$\frac{d\upsilon}{d\xi} = (0.75/\sqrt{\pi}) \exp(-0.563\xi^2) \tag{30}$$

with

$$\xi = \frac{1.93d}{d_{max}-d}. \tag{31}$$

The above correlation for the droplet size distribution implies that the distribution can be uniquely determined by the maximum stable diameter which is a function of the gas and liquid properties and their respective flow rates as indicated by the correlation for d_{max} given by equation (21).

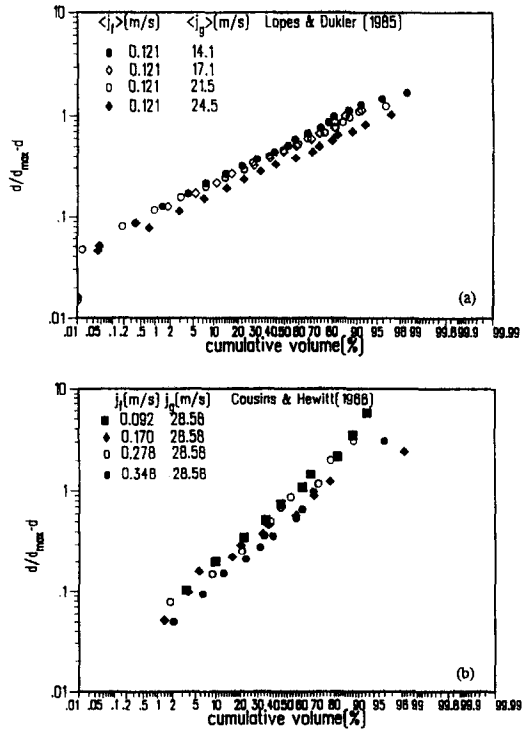

FIG. 3. Example of upper limit, log-normal distribution: (a) Lopes and Dukler [3]; (b) Cousins and Hewitt [17].

Mean droplet sizes

By knowing the droplet size distribution, one may calculate expressions for the mean diameters according to the upper-limit log-normal distribution. The Sauter mean diameter, d_{32} and the volume median diameter, d_{vm}, can be easily derived in terms of the maximum stable droplet diameter. They are given by

$$d_{max}/d_{vm} = 2.93 \quad \text{and} \quad d_{max}/d_{32} = 4.01. \tag{32}$$

These equations can be used together with d_{max} correlation given by equation (21) to derive expressions for d_{vm} and d_{32}. They are given in dimensionless form as follows:

$$d_{vm}/d_h = 0.90C_w^{-4/15} We_m^{-3/5} (Re_g^4/Re_f)^{4/15} \times [(\rho_g/\rho_f)(\mu_g/\mu_f)]^{4/15} \equiv 0.90K \tag{33}$$

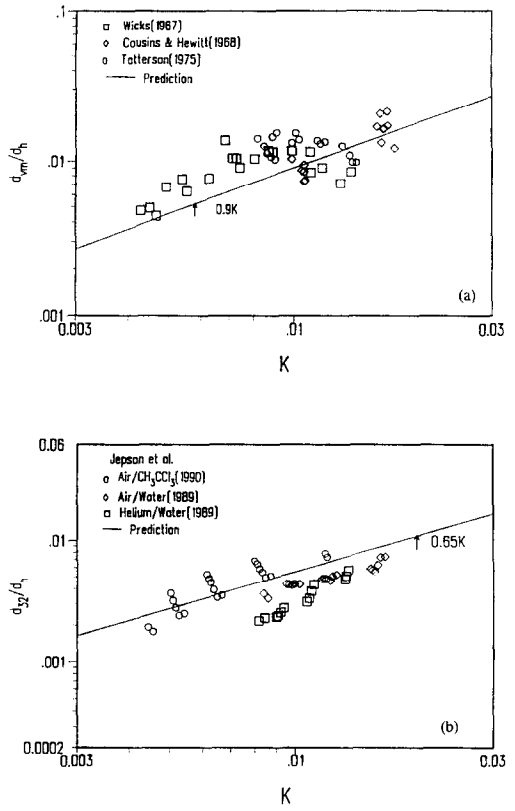

FIG. 4. Theoretical and experimental values of Sauter mean diameters: (a) volume median diameter; (b) Sauter mean diameter.

and

$$d_{32}/d_h = 0.64C_w^{-4/15}\,We_m^{-3/5}\,(Re_g^4/Re_f)^{4/15} \times [(\rho_g/\rho_f)(\mu_g/\mu_f)]^{4/15} \equiv 0.65K. \quad (34)$$

The above equations are compared with experimentally measured mean diameters of several investigators [5, 6, 12–14] in Figs. 4(a)–5(c). The conditions of these experiments are described in Table 1. Figure 4(a) illustrates such a comparison in terms of the volume median diameters whereas Fig. 4(b) shows a comparison in terms of the Sauter mean diameter. Figures 5(a)–(c) illustrate more detailed comparison with Jepson *et al.* data covering a wide range of physical properties of fluids.

The Cousins and Hewitt data compare fairly well with predictions. Wicks' data are consistently underestimated by the present correlation in the range of lower values of K in Fig. 4(a). However, a systematic similarity in tendency between predictions and measurements of d_{vm} is a strong indication that the mechanistic model used here to derive the maximum stable droplet size properly accounts for the essentials of the droplet break-up process. Tatterson's data show much higher spread with the measurement of d_{vm}. There may be several reasons for the apparent but consistent discrepancies.

(1) Still photography was used by Cousins and Hewitt for upward flow of air and water in a circular channel of 9.5 mm. Wicks [14] and Wicks and Dukler [15] used an electrical conduction probe technique for the downward flow of air and water in a rectangular channel, 150 mm wide and 19 mm deep. The probe consists of two needles pointing at each other in the air stream containing droplets. By varying the spacing between the needle tips, the functionality between the counting rate and distance of separation was determined, and the drop size distribution was extracted from these results by numerical methods. Tatterson applied an electrical probe technique to measure drop sizes for air/water flow in a horizontal rectangular channel 25 mm deep and 305 mm wide. The signal from the probe was analyzed electrically to get the drop size distribution. From these experimental techniques, those based on photographic data are certainly the most reliable. The probe techniques used by Wicks and Tatterson consistently yield higher droplet sizes as compared to the predictions.

(2) Both Wicks' and Tatterson's experimental test section consisted of rectangular channels. One possibility of the apparent but consistent disagreement on the d_{vm} is that the interfacial shear used for the present correlation might not have been proper for the rectangular flow channels. However, as the mechanistic model implies, the similarity in tendency would indicate that the drop size is not very sensitive to the flow orientation.

(3) As demonstrated by Lopes and Dukler [3], the place where the droplet size sampling is made in the annular core is very important in the droplet size measurements since the average drop size decreases towards the center of the annular two-phase column. It is evident, therefore, that any droplet size measurement close to the interface will yield higher average droplet sizes. This may also be an important factor for the obvious but consistent disagreement shown in Fig. 4(a).

The overall agreement in Fig. 4(b) is particularly encouraging since the experiments cover a large range of physical property group from 540 to 3700 for (ρ_f/ρ_g) and the modified Weber number group from 125 to 3285. Considering the experimental uncertainties involved in the droplet size measurements, the predicted mean droplet sizes agree reasonably well with those measured sizes. This indicates that the principle mechanisms involved in the droplet break-up process were properly accounted for in the development of the theoretical model.

Figures 5(a)–(c) compare the predicted dependence of the Sauter mean drop diameter on liquid and gas Reynolds number with the drop size data for the fluid systems air/CH_3CCl_3, air/water and He/water. All systems show the drop size decreasing with increasing gas Reynolds number as predicted. However, there is a general disagreement in terms of the liquid Reynolds number dependence. The experimental observations

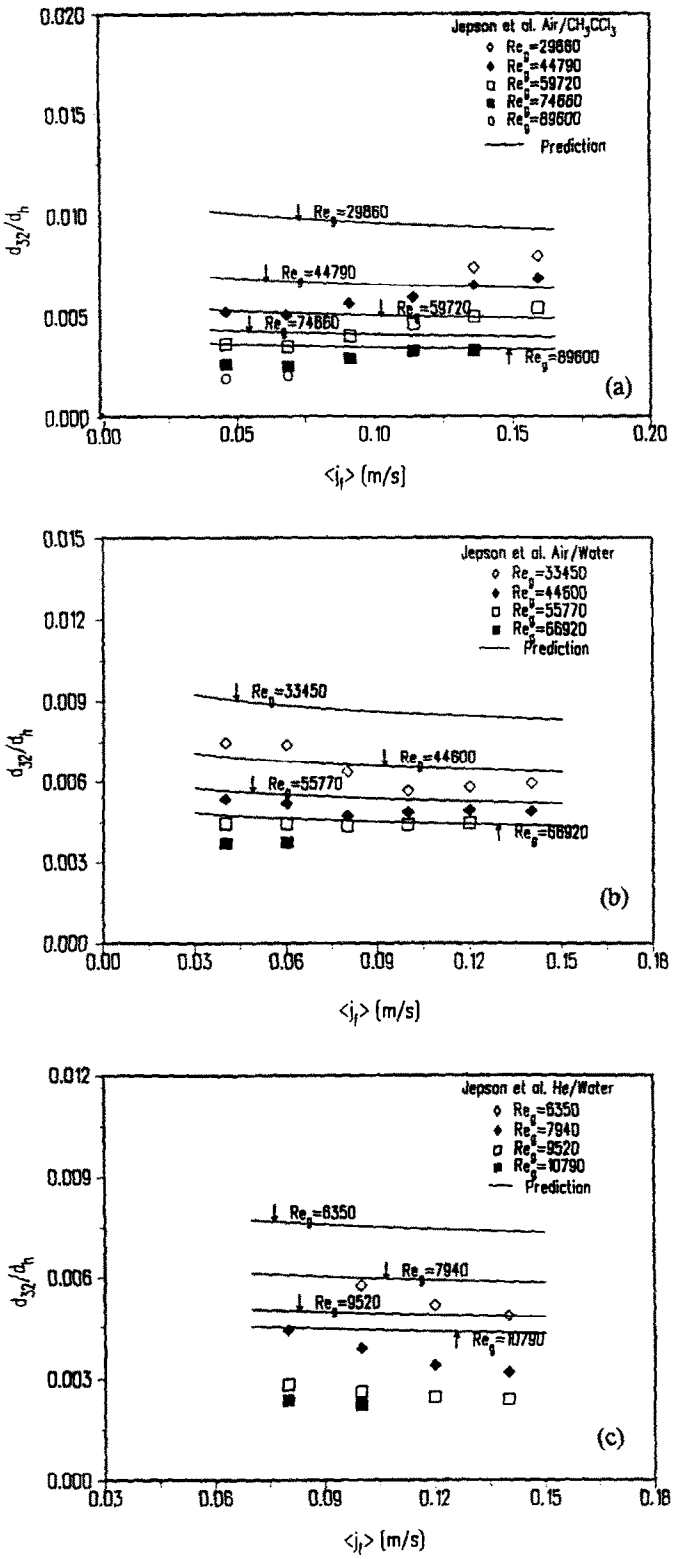

FIG. 5. Comparison between predicted and measured Sauter mean diameters: (a) air/CH_3CCl_3 data, Jepson *et al.* [5]; (b) air/water data, Jepson *et al.* [5]; (c) He/water data, Jepson *et al.* [6].

Table 1. Summary of various experiments on droplet mean diameters

Source	Fluids	Flow channel	Flow direction	Experimental technique	$Re_g \times 10^{-3}$	$Re_f \times 10^{-3}$	We_m	ρ_f/ρ_g	μ_f/μ_g	$N\mu \times 10^3$
Wicks and Dukler [15], Wicks [14]	Air/Water	19 × 150 mm channel (d_h = 33.7 mm)	Vertical down	Electrical conductance	66–170	0.75–3.9	320–4100	750	54	2.24
Cousins and Hewitt [17]	Air/Water	9.5 mm ID tube	Vertical up	Photographic	36–62	0.60–4.0	276–850	420	54	2.24
Tatterson [16]	Air/Water	25 × 30.5 mm channel (d_h = 46.2 mm)	Horizontal	Electrical conductance	101–182	0.85–3.9	880–2900	725	54	2.24
Lopes and Dukler [3]	Air/Water	50.74 mm ID tube	Vertical up	Laser optical	52–96	1.7–7.0	180–560	760	54	2.26
Jepson *et al.* [5]	Air/Water	10.26 mm ID tube	Vertical up	Laser diffraction	22–67	0.41–1.5	125 ~ 1130	555	54	2.24
Jepson *et al.* [6]	He/Water	10.26 mm ID tube	Vertical up	Laser diffraction	63–108	0.41–1.5	75–218	3700	52	2.24
Jepson *et al.* [5]	Air/CH_3CCl_3	10.26 mm ID tube	Vertical up	Laser diffraction	26–78	0.92–1.8	365–3285	540	50	4.17

of Jepson *et al.* indicate that for increasing Re_f, the Sauter mean diameter shows a minimum for air/water system, a continuous decrease with He/water and an increase for air/CH_3CCl_3 system, whereas the predictions show a slight decrease with Re_f. As discussed in the Mechanistic Modeling of Droplet Break-up section, this apparent disagreement may be attributed to the insensitivity of the interfacial shear stress, τ_i, to the different entrainment mechanisms and of the droplet volumetric concentration. It is believed that both of these factors play important roles in determining the mean droplet size in an annular flow. More specifically, mechanistic interfacial shear expressions which can be used for a wide range of flow variables are needed. Presently an analytical study is underway to clarify the above disagreements.

SUMMARY AND CONCLUSIONS

Two Weber number criteria, one based on the classical Kolmogorov theory and the other on Levich's theory, were discussed and compared to each other. It was concluded that when $\rho_d \leqslant \rho_c$, the entrainment of fluid particles by turbulence may be complete, and that Weber number criterion based on Kolmogorov's theory mechanistically describes the fragmentation of drops and bubbles in a turbulent liquid flow. However, in the case of droplets in a gas stream with $\rho_d \gg \rho_c$, the entrainment of droplets by turbulent eddies cannot be complete, and relative motions play a major role instead of eddies in the mechanism of droplet disintegration.

Based on the competing stresses between stabilizing surface forces and disruptive dynamic forces, a theoretical model was developed to describe the break-up of entrained droplets in the gas core of an annular flow. The experimental data of the maximum droplet size were correlated in terms of Re_g, Re_f, We_m, and the physical property groups of (ρ_f/ρ_g), (μ_f/μ_g) and $N\mu$. Effects of each group in determining the maximum stable droplet size were discussed in the context of available experimental data. It was concluded that the functional dependence of d_{max} on these groups could be experimentally verified. Contradictory experimental data on pipe size and liquid flow dependency indicate that drop size measurements with a larger range of flow channel sizes and of liquid flow rates would, however, be desirable in order to test further the proposed mechanism and the method outlined to predict droplet size. In particular, it is essential to obtain more and more detailed data on droplet size at various portions after droplet entrainment.

An upper limit log-normal volume distribution function was fitted to the experimental data with distribution parameters $a = 1.93$ and $\eta = 0.75$. Based on these parameters, predictive equations were developed for the most representative mean droplet sizes, the volume median diameter and Sauter mean diameter. The predicted mean droplet sizes were found to agree

reasonably well with those measured mean sizes. This indicates that the principal mechanisms involved in the droplet break-up process in a turbulent gas stream were properly accounted for in the development of the theoretical model.

Acknowledgements—This work was supported by the U.S. Department of Energy, Office of Basic Energy Science under Grant D. E. FG02-87ER13764. The authors would like to express their sincere appreciation for the encouragement, support and technical comments on this program from Dr O. P. Manley of the U.S. DOE/BES.

REFERENCES

1. I. Kataoka, M. Ishii and K. Mishima, Generation and size distribution of droplet in annular two-phase flow, *J. Fluid Engng* **105,** 230–238 (1983).
2. P. B. Whalley, G. F. Hewitt and J. W. Terry, Photographic studies of two-phase flow using a parallel light technique, UKAEA Report, AERE-R9389 (1979).
3. J. C. B. Lopes and A. E. Dukler, Droplet sizes, dynamics and deposition in vertical annular flow, University of Houston Report, NUREG/CR-4424 (1985).
4. A. N. Kolmogorov, On the disintegration of drops in a turbulent flow, *Doklady Akad. Nauk., SSSR* **66,** 825–833 (1949).
5. D. M. Jepson, B. J. Azzopardi and P. B. Whalley, The effect of gas properties on drops in annular flow, *Int. J. Multiphase Flow* **15,** 327–339 (1989).
6. D. M. Jepson, B. J. Azzopardi and P. B. Whalley, The effect of physical properties on drop size in annular flow, *Proc. Ninth Int. Heat Transfer Conf.*, Vol. 6, pp. 95–100 (1990).
7. G. I. Taylor, The formation of emulsion in definable field of flow, *Proc. Royal Soc. (Lon.)* **A164,** 501–507 (1934).
8. G. K. Batchelor, Pressure fluctuations in isotropic turbulence, *Proc. Cambridge Phil. Soc.* **47,** 359–374 (1951).
9. V. G. Levich, *Physicochemical Hydrodynamics*. Prentice Hall, Englewood Cliffs, New Jersey (1962).
10. M. Sevik and S. H. Park, The splitting of drops and bubbles by turbulent fluid flow, *J. Fluids Engng* **95,** 53–59 (1973).
11. J. O. Hinze, Fundamentals of the hydrodynamic mechanism of splitting dispersion processes, *A.I.Ch.E. Jl* **1,** 289–295 (1955).
12. M. Ishii and M. A. Grolmes, Inception criteria for droplet entrainment in two-phase concurrent film flow, *A.I.Ch.E. Jl* **21,** 308–316 (1975).
13. G. B. Wallis, *One Dimensional Two-Phase Flows*. McGraw-Hill, New York (1969).
14. M. Wicks, Liquid film structure and drop size distribution in two-phase flow, Ph.D. Dissertation, University of Houston, Houston, Texas (1967).
15. M. Wicks and A. E. Dukler, In situ measurements of drop size distribution in two-phase flow, a new method for electrically conducting liquids, *Int. Heat Transfer Conf.*, Chicago, Illinois (1966).
16. D. F. Tatterson, Rates of atomization and drop size in annular two-phase flow, Ph.D. Dissertation, University of Illinois, Illinois (1975).
17. L. B. Cousins and G. F. Hewitt, Liquid phase mass transfer in annular two-phase flow: droplet deposition and liquid entrainment, UKAEA Report, AERE-R5657 (1968).
18. R. D. Linstead, D. L. Evans, J. Gass and R. V. Smith, Droplet and flow pattern data, vertical two-phase (air-water) flow using axial photography, Wichita State University, Department of Mechanical Engineering (1978).
19. J. T. Pogson, J. H. Roberts and P. J. Whibler, An investigation of the liquid distribution in annular-mist flow, *J. Heat Transfer* **92,** 651–658 (1970).
20. B. J. Azzopardi, G. Freeman and D. J. King, Drop sizes and deposition in annular two-phase flow, UKAEA Report, AERE-R9634 (1980).
21. B. J. Azzopardi, G. Freeman and P. R. Whalley, Drop sizes in annular two-phase flow, UKAEA Report, AERE-R9074 (1978).
22. B. J. Azzopardi, S. Taylor and D. B. Gibbons, Annular two-phase flow in a large diameter tube, *Proc. Int. Conf. on the Physical Modelling of Multi-Phase Flow*, BHRA Fluid Engineering, Coventry, England (1983).
23. G. Kocamustafaogullari, W. D. Huang and J. Razi, Measurement and modeling of average void fraction, bubble size and interfacial area, *J. Nucl. Engng Design* (in press).
24. T. Ueda, Entrainment rate and size of entrained droplets in annular two-phase flow, *Bull. JSME* **22,** 1258–1265 (1979).
25. S. Namie and T. Ueda, Droplet transfer in two-phase annular mist flow, *Bull. JSME* **15,** 1568–1565 (1972).
26. D. F. Tatterson, J. C. Dallman and T. J. Hanratty, Drop sizes in annular gas–liquid flows, *A.I.Ch.E. Jl* **23,** 68–76 (1977).
27. R. A. Mugele and H. D. Evans, Droplet size distribution in sprays, *Ind. Engng Chem.* **43,** 1317–1324 (1951).
28. P. Andreussi, G. Romero and S. Zanelli, Drop size distribution in annular-mist flows, *First Int. Conf. on Liquid Atomization and Spray Systems*, Tokyo, Japan (1978).